PARTICLE IMAGE VELOCIMETRY MEASUREMENT INSIDE AXIAL AIR TEST TURBINE

D. Duda, V. Yanovych, V. Uruba, P. Žitek
University of West Bohemia in Pilsen

M. Němec, T. Jelínek
Czech Aerospace Research Centre in Prague

ABSTRACT

We measure the two dimensional instantaneous velocity fields inside an axial turbine by using the technique PIV (Particle Image Velocimetry). The measured plane is located just behind the rotor wheel and it is oriented in axial × tangential direction. We measured a single overloaded regime as well as the nominal one at tip radius. We discuss several technical difficulties appearing during this measurement, mainly with the seeding particles and with the optical access into a massive steel body. The glass dividing the channel past rotor and the empty space of diffusor has been dirtied by large oil droplets condensing at the blades and splashed to this window. We "solved" this trouble by removing the glass, because it anyway divides volumes with same static pressure. Best quality result was obtained without this glass, but its removal changes the geometry. In our contribution we focus to the effect of such rude change to the trustworthiness of the results.
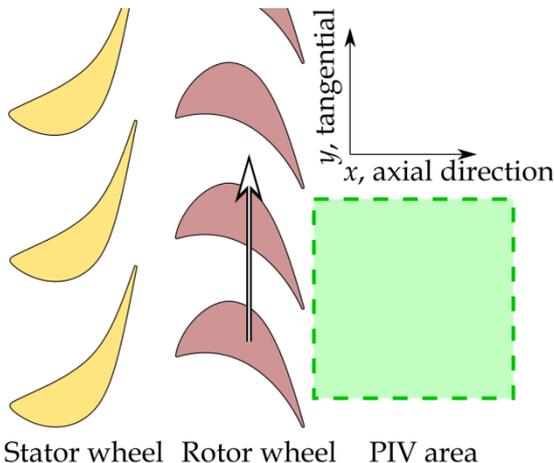
Figure 0: Sketch of the studied PIV area just behind the rotor wheel. The air flows from left to right. The field of view has size 28 mm.

NOMENCLATURE

PIV   Particle Image Velocimetry
I_T Turbulence intensity
u Axial velocity component
v Tangential velocity component
w Magnitude of velocity (radial component is not measured)
Ma   Mach number
α Velocity angle relative to axial direction
σ Standard deviation

INTRODUCTION

Among the variety of methods for measuring flow velocity, the technique of Particle Image Velocimetry (PIV) [1] offers the *spatial resolution* of the instantaneous velocity field, which is advantageous for studying the coherent structures of turbulence. The ensemble of such instantaneous velocity fields serves for both, the studies of the average flow pattern as well as for the fluctuation structures of Reynolds decomposed velocity fields [2]. PIV is an optical method, therefore it does not disturb the flow by any probe, but on the other hand, it needs seeding particles, whose motion is measured. The need of optical access from two directions (for illumination laser and for camera) makes its use difficult for in-situ measurements. Another disadvantage is the slow laser charging limiting the temporal resolution far under the typical time of the flow. This disadvantage can be partly canceled by the synchronization of the PIV system with the rotation the rotor, which results into set of instantaneous velocity fields, which are not correlated in time, but in the phase of the periodically driven flow.

This is the reason, why the majority of engineering hydrodynamic studies are performed by using pressure probes [1], whose robustness and quite straightforward interpretation (only the knowledge of fluid density is needed) make them the first choice for in-situ testing. But, the pressure probe needs to be pointed directly against the main flow and, when the angle is not known or it is a subject of investigation, then a multihole probe with quite complicated calibration procedure has to be used.

There exist more of the so-called point methods (it does not refer to the fluid point, with size smaller than Kolmogorov length, but to the fact, that their results have form of a single number representing the entire probed volume) with or without the temporal resolution. The mentioned

pressure probes typically do not offer the fine temporal resolution, only is the pressure transducer is very close to the hole. The imaginary king in the time resolution is the Hot Wire Anemometry method (sometimes referred as Constant Temperature Anemometry) [1], with sampling frequency going into hundreds of kilohertz. On the other hand, the wire itself is very fragile and has a limited lifetime.

The turbomachinery hydrodynamics is mostly studied by pressure methods; deeper studies use Hot Wire Anemometry [3].

EXPERIMNTAL SETUP

The test facility at the Czech Aerospace Center consists of single stage axial air turbine, the hydraulic dynamometer and powerful 12-stages air compressor. This facility serves mainly for measuring integral characteristics of different rotor and stator wheels under large scale of conditions. While the measurement with pressure probes is quite common here, the optical methods need a new access into the turbine.

The PIV (Particle Image Velocimetry) technique is based on observing the motion of small particles carried by the flow. These particles are illuminated by a double-pulsed solid state laser with beam defocused in one direction by a cylindrical lens (in fact it is more lenses) resulting into a planar laser-sheet of thickness about 1 mm and width in order of tens or hundreds of mm in dependence on distance from aperture. We use the NewWave Solo laser with pulse energy up to 500 mJ. The particle positions are captured by using a camera, which can distinguish two expositions separated by only few microseconds (5 µs in the present data). We use the Mk II FlowSense 4 MPix camera.

The optical access for laser beam is localized in the diffusor body by window in the cylindrical steel wall. The laser is oriented perpendicularly to the turbine axis and the laser sheet is mirrored into the counter-axial direction by using a planar mirror mounted on a computer-controlled linear traverser, which allow changing the explored radius. In this contribution we present only data taken at the tip radius.

The optical access for camera is made in the cylindrical body axially just behind the rotor wheel. There are two windows due to the presence of a cylindrical wall, which is a removable insert allowing installation of different size wheels into the test turbine.

The synchronization of PIV system and rotor wheel rotations allow to study the average pattern of the rotor wake. The instantaneous data show large amount of vortices of size about the shear layer thickness and the spatial spectrum follow the Kolmogorov scaling for homogeneous and isotropic turbulence under that size.

We had several troubles with the condensation of seeding particles on the glass between the diffuser and main body. Best quality result was obtained without this glass, but its removal changes the geometry. In our contribution we focus to the effect of such rude change to the trustworthiness of the results.

RESULTS – NOMINAL REGIME

Figure 1 shows the in-plane angle of average velocity in respect to the axial direction:

$$\alpha = \operatorname{atan} \frac{v}{u}$$

where u and v are the axial and tangential velocity components respectively. Note that there is important first to average, second to calculate the angle, as the atan function is non-linear, therefore averaging instantaneous angles gives different result than angle of average velocity.
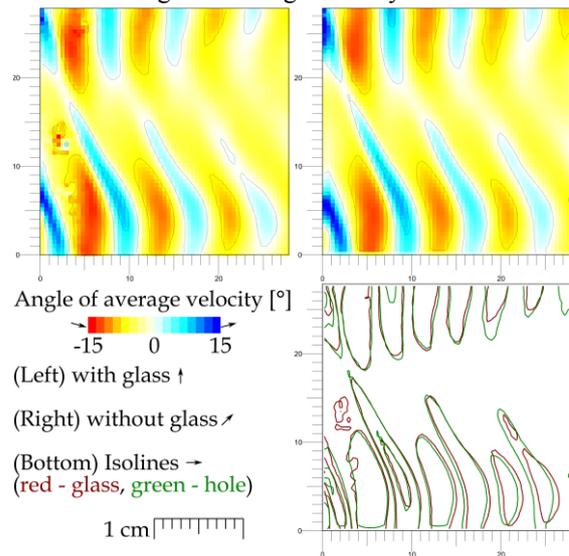

Angle of average velocity [°]

-15   0   15

(Left) with glass ↑

(Right) without glass ↗

(Bottom) Isolines →
(red - glass, green - hole)

1 cm

Figure 1: Angle of ensemble (600 snapshots) averaged velocity. The angle is relative to the axial direction. The data are taken at tip radius at Mach number Ma = 0.40 and under nominal conditions.

The average flow pattern has a form of alternating approximately vertical strips faster and slower fluid (Figure 2) corresponding to jets and wakes past the rotor wheel (wakes past the blades, jets past the inter-blade channels). In the shear layers between jets and wakes, the average flow direction is deflected in the tangential direction (Figure 1). These strips are partially overlapped by horizontal wakes (~ upper half of field of view) and jets (~ bottom half of field of view) caused by the stator wheel preceding the rotor. We can see that the inhomogeneity of flow angle caused by rotor blades is less disturbed in the shear layer between the wake and jet of stator. The deflection of flow angle signifies the fluid still contain some momentum, which has not been transferred to the rotor and thus this energy is escaping the turbine. The spatial average and standard deviation of angle of (temporal) average velocity is -3.2° ± 4.8° for

the case without glass, while it is -3.5° ± 4.5° with glass.

The inner glass closing the hole in the diffusor body causes serious troubles due to oil droplets decreasing transparency and causing spurious reflections. These reflections from large droplets slowly traveling on the glass are a big problem as they move and thus cannot be subtracted. Their effect is visible even in average data – see the left part of Figure 1, where a spurious spot of differently oriented velocity shines. The higher moments are naturally even more sensitive to such disturbances.

Due to the lack of measuring time during this quite complicated campaign, we "solved" this issue simply by removing the problematic part. The quality of resulting data is much better, as can be seen in Figure 1 right, but, on the other hand, it changes the geometry significantly! Fortunately, the static pressure on both sides of the inner body (which in fact only serves for fitting different radii wheels into the test facility) is same. Therefore, the flow might not be affected much. To answer this important question, we compare data at both variants in light of isolines (or contour lines) of several average quantities.
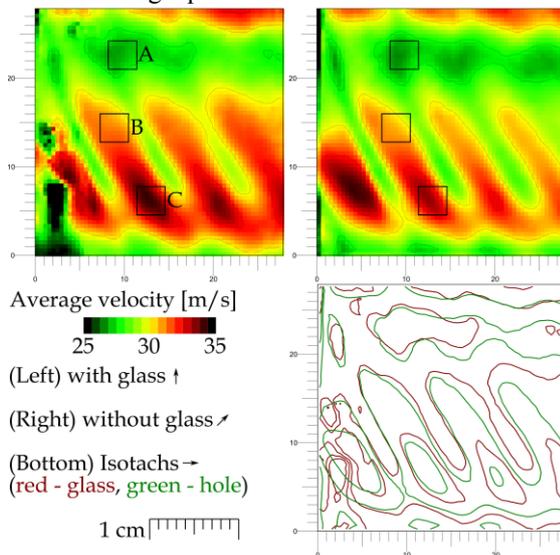

Figure 2a: Magnitude of average velocity. The legend spans ± 5 m/s around the average magnitude (which is measured to be 29.9 and 29.5 m/s respectively). Black rectangles highlight cross-section of stator and rotor wake (A), that of stator and rotor jet (C) and the area of minimal turbulence (B); they will be discussed later. The data are taken at tip radius at Ma = 0.40 and under nominal conditions.

The magnitude w displayed in Figure 2 is calculated by using the in-plane velocity components only (they are measured):

$$w = \sqrt{u^2 + v^2}$$

In this plot we can see the effect of widening of the flow path in the case with hole in the outer

cylindrical body: the right parts of the fields of view display systematically lower velocity magnitude (greener colors) in the case with hole.
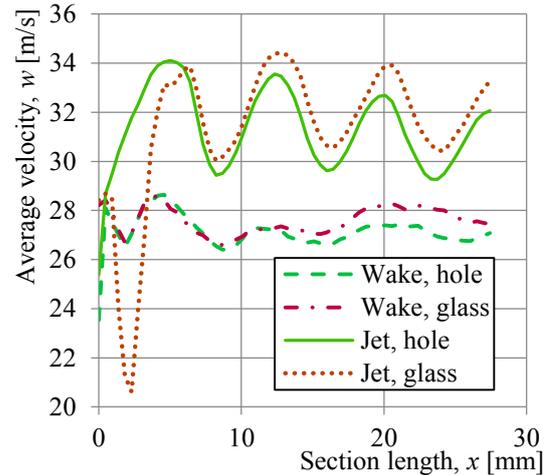

Figure 2b: Magnitude of average velocity along axial sections following jet (y-position of C region) and wake (y-position of A region) respectively.

This effect is better apparent when comparing the sections of this data, see Figure 2b Still the effect of artificial hole in the outer cylindrical wall is smaller than the inhomogeneity of the velocity caused by the stator wheel. It is interesting, that the height of velocity peaks associated with rotor system is larger in the stator jet, than in the stator wake.
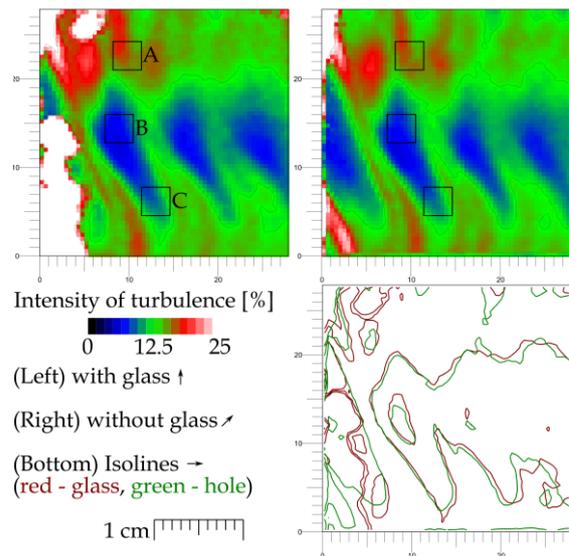

Figure 3: Turbulence intensity calculated by using the in-plane components (it is underestimated by the radial components and by the fluctuations of length-scale smaller than the experimental resolution). The data are taken at tip radius at Mach number Ma = 0.40 and under nominal conditions.

The turbulence intensity is defined historically as the ratio of standard deviation of velocity to its average value

$$I_T = \frac{\sigma[u]}{\langle u \rangle}$$

but, we have to note, that this definition is prepared for typical one-dimensional point method with average drift velocity significantly larger than the fluctuations. PIV is not limited by this requirement and it is two-dimensional method. Thus we rather use the definition with energies, which for 1D case converge to the definition above:

$$I_T = \sqrt{\frac{\langle u^2 \rangle - \langle u \rangle^2 + \langle v^2 \rangle - \langle v \rangle^2}{\langle u \rangle^2 + \langle v \rangle^2}}$$

Turbulence intensity represents the amount of energy, which is already removed from the main flow, and it has the form of mechanical energy still, but with higher entropy – it occupies smaller length-scales and it is not organized regularly in time. An interesting question asks, in which direction the velocity fluctuates more [4]. It is generally known [5, 6], that in the case of wake flows, the stream-wise fluctuations are stronger in the shear layer at the wake boundary, but in the center of the wake, there dominate the span-wise fluctuations.
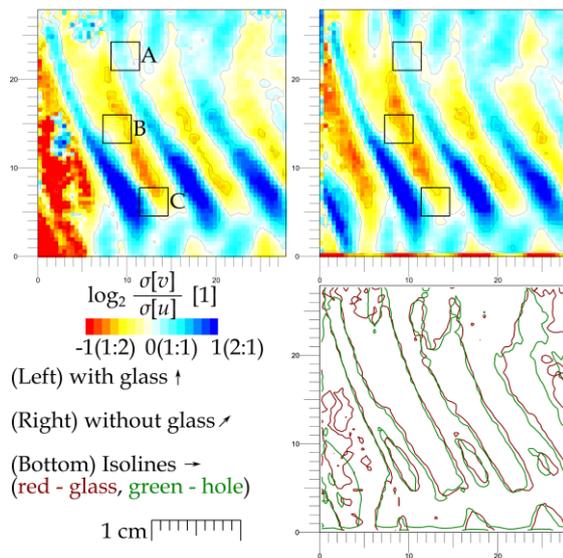

Figure 4: Anisotropy of fluctuations in light of ratio of fluctuations in the tangential to the axial direction [4]. Logarithm is advantageous for this quantity, because it maps the interval [0, ∞] with center in 1 (fluctuations same in both directions) to symmetric interval [-∞, ∞] with center in 0 (i.e. -∞ corresponds to all fluctuations in axial direction, +∞ does for all in tangential direction, -1 means that there is 2× more fluctuations in axial direction than in tangential one and +1 does oppositely).

Our findings according to 2D isotropy (for the full insight into the isotropy of fluctuations we would need the Stereo PIV data [7], which is planned for future) are shown in Figure 4, where we compare the amount of fluctuations in tangential and axial direction. The topology of this

ratio follows the spatial distribution of velocity angle (Figure 1).
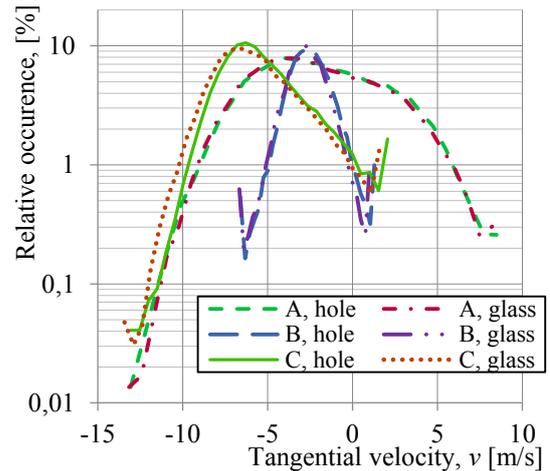
STATISTICS OF TANGENTIAL VELOCITY

Figure 5: Histogram of instantaneous tangential velocity component in three depicted regions. The vertical axis is in logarithmic scale and it is normalized by the number of points; the horizontal axis is linear and not normalized in order to show different means as well. The first and last point of each line contains events out of the interval. Each line contains 29400 datapoints.

In Figure 2a we depicted three regions of interest; first (A) lies in the cross-section of stator a rotor wakes, the magnitude of average velocity is minimal there; second (B) is area of minimal intensity of turbulence (compare with Figure 3) and the third (C) displays maximum magnitude of average velocity. We show the statistics of tangential velocity component in these regions in Figure 5.
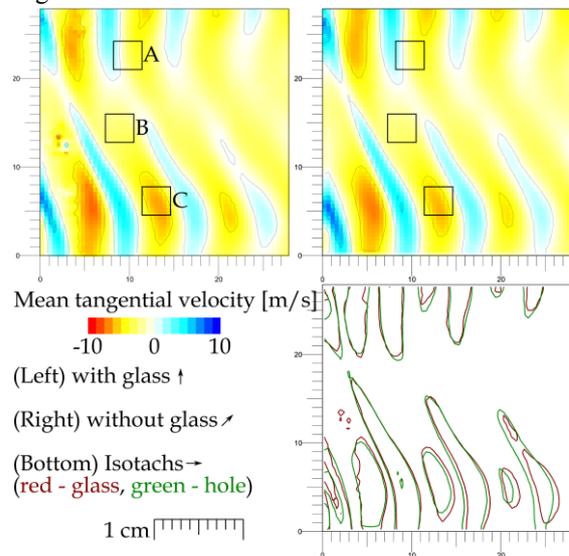

Figure 6: First statistical moment (i.e. average) of tangential velocity v.

Tangential velocity component is important from the energetic point of view, because it carries

out the angular momentum, which cannot be used as a turbine work. Inside a mysterious ideal turbine, the outgoing tangential velocity might be zero at all positions and at all times.

The first statistical moment is just an ensemble average. Its topology is very similar to that of angle of average velocity (compare Figures 6 and 1).
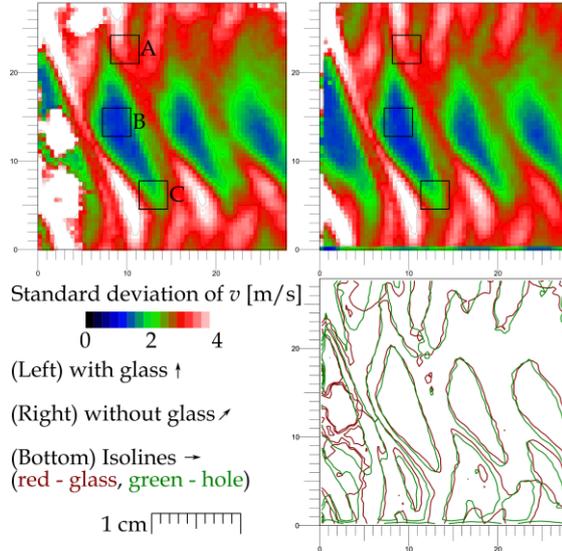

Standard deviation of v [m/s]

0   2   4

(Left) with glass ↑

(Right) without glass ↗

(Bottom) Isolines →
(red - glass, green - hole)

1 cm

Figure 7: Second statistical moment (i.e. standard deviation) of tangential velocity v.

The second statistical moment is called standard deviation σ and it is calculated as
$$\sigma[v] = \langle (v - \langle v \rangle)^2 \rangle = \langle v^2 \rangle - \langle v \rangle^2$$
Its pattern is very similar to that of turbulence intensity (Figure 3), because turbulence intensity consists partly of this quantity and, at the same time, the ratio of axial and tangential fluctuations does not departs much from isotropy (see Figure 4).
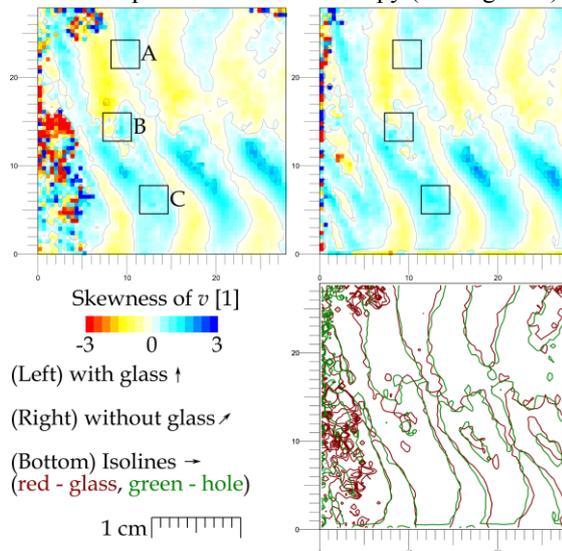

Skewness of v [1]

-3   0   3

(Left) with glass ↑

(Right) without glass ↗

(Bottom) Isolines →
(red - glass, green - hole)

1 cm

Figure 8: Third statistical moment (i.e. skewness) of tangential velocity v.

The third statistical moment, called *skewness*, shows the left-right anisotropy of strong rare events. In other words, the negative skewness tells,

that there are few events much smaller than the mean, which are balanced by higher number of events not so larger than the mean. Positive value means oppositely. Skewness is calculated as
$$S[v] = \frac{\langle (v - \langle v \rangle)^3 \rangle}{\sigma^3[v]}$$
therefore, it is a dimensionless quantity. As the moment rises, the result is much more sensitive to the noise (it focuses to rare events far from average), thus also the plot of S is less visually attractive than some mean quantities.
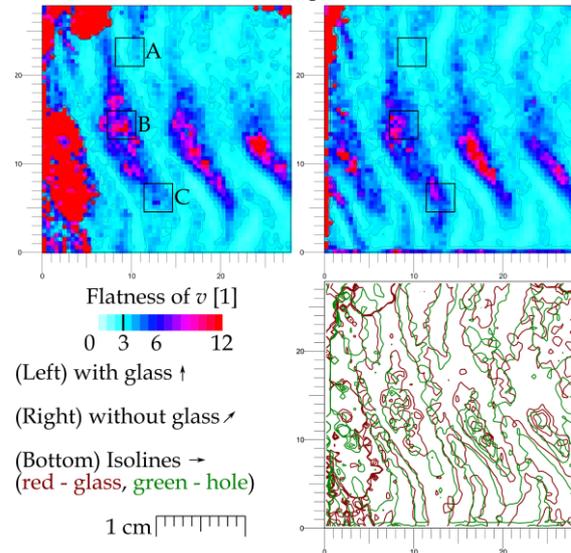

Flatness of v [1]

0   3   6   12

(Left) with glass ↑

(Right) without glass ↗

(Bottom) Isolines →
(red - glass, green - hole)

1 cm

Figure 9: Forth statistical moment (i.e. flatness) of tangential velocity v. Flatness of a Gaussian distribution is equal to 3, which is depicted in the legend and it is the level of one isoline.

Flatness is the fourth statistical moment calculated as
$$F[v] = \frac{\langle (v - \langle v \rangle)^4 \rangle}{\sigma^4[v]}$$
it is very sensitive to strong rare events (and naturally to the noise as well). Physically, it is interpreted as a sign of intermittency. It is typically produced in the areas with generally quiet flow, which are time-to-time visited by a turbulent patch from the neighboring more wild regions. Look to region B, where F is high, while σ is low. Similarly in the histogram plot (Figure 5), region B displays narrow distribution with high out-of-interval peaks.

RESULTS – OVERLOADED REGIME

The off-design regimes are very important in nowadays, when the instability caused by so-called green energy resources has to be compensated in classical steam turbines, which are then forced to work during significant periods in off-design regimes.

The overloaded regime occurs when the breaking force acting to the rotor wheel slows its velocity under the ideal one; direct consequence is the non-axial direction of fluid leaving the stage, which carries a relevant amount of axial momentum, i.e. energy which is not transferred to

5

the mechanical energy of the rotor. In this measurement, we tested the overload regime with ratio of rotor speed to the axial fluid velocity equal to 0.4 (remember this ratio at nominal regime is 0.55).
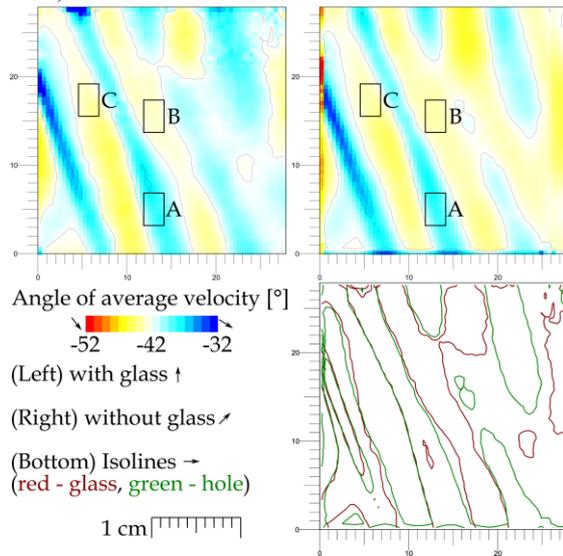

Angle of average velocity [°]

-52   -42   -32

(Left) with glass ↑

(Right) without glass ↗

(Bottom) Isolines →
(red - glass, green - hole)

1 cm

Figure 10: Angle of average velocity. The data are taken at tip radius at Mach number Ma = 0.40 and at overloaded regime with wheel-to-fluid ratio 0.40.

The measured spatial average of angle of ensemble-average fluid velocity is -41.3° ± 2.2° with the problematic covering glass, or it is measured to be -42.0° ± 2.3° without this glass.

Average velocity [m/s]

35   42.5   50

(Left) with glass ↑

(Right) without glass ↗

(Bottom) Isotachs →
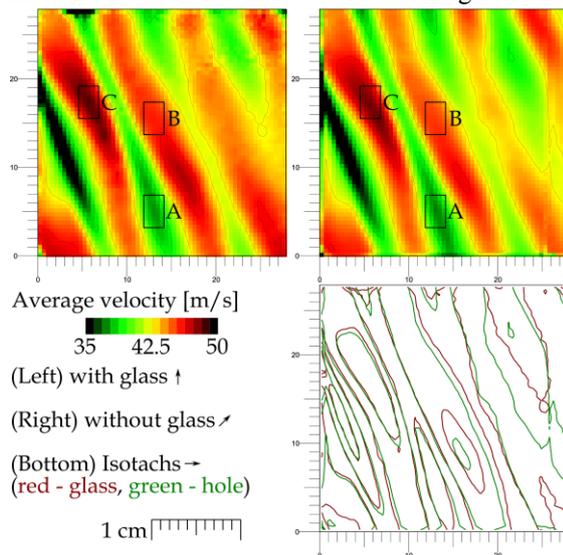(red - glass, green - hole)

1 cm

Figure 11: Magnitude of average velocity. The data are taken at tip radius at Mach number Ma = 0.40 and at overloaded regime with wheel-to-fluid ratio 0.40.

The topology, again, consists of system of wakes and jets past rotor wheel and a similar system past stator wheel, which is parallel with the average flow (stator is static). Therefore, the overlap regions of stator jet with rotor jet or stator

wake with stator wake are larger and thus they can contain also larger turbulent structures. Larger structures contain more energy and thus also the energy dissipation is larger than under nominal conditions.

The overloaded regime is much more affected by the droplets splashed onto the window, which is most apparent at the distribution of higher moments, e.g. the turbulence intensity in Figure 12. The quality of data is not high, thus we had to use a filtering algorithm based on the energy content at lowest resolved length scale described in our article [8]. On the other hand, the overloaded regime seems to be more sensitive to the geometry change caused by removing the glass leaving a hole in its place. This is logic, when we take into account the non-zero tangential motion of the fluid and the consecutive centrifugal force.
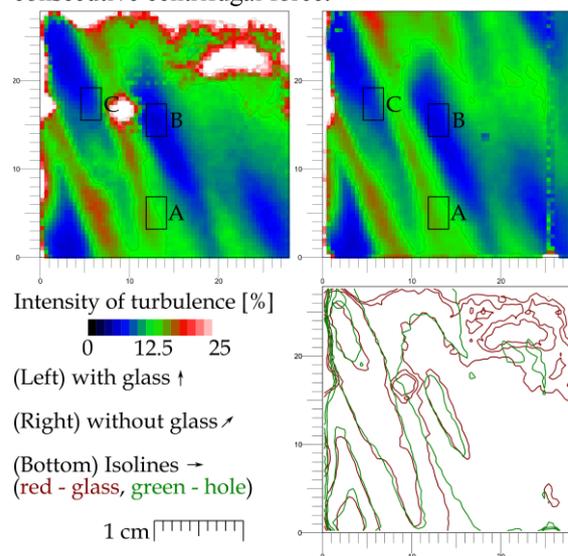

Intensity of turbulence [%]

0   12.5   25

(Left) with glass ↑

(Right) without glass ↗

(Bottom) Isolines →
(red - glass, green - hole)

1 cm

Figure 12: Turbulence intensity. Note the clearly apparent individual droplets apparent as spots of diverging I_T. The data are taken at tip radius at Mach number Ma = 0.40 and at overloaded regime with wheel-to-fluid ratio 0.40.

While the field of view was affected by the splashed droplets most in its left part under the nominal condition, at the overloaded regime, it contains more noise in its upper part − compare Figures 3 and 12 plotting the turbulence intensity.

The ratio of intensities of fluctuations in the tangential to that in the axial direction does not make sense in the areas disturbed by some droplets, but elsewhere it displays quite a good agreement between the two discussed cases as well as with the topology of the angle distribution, which has been argued previously.
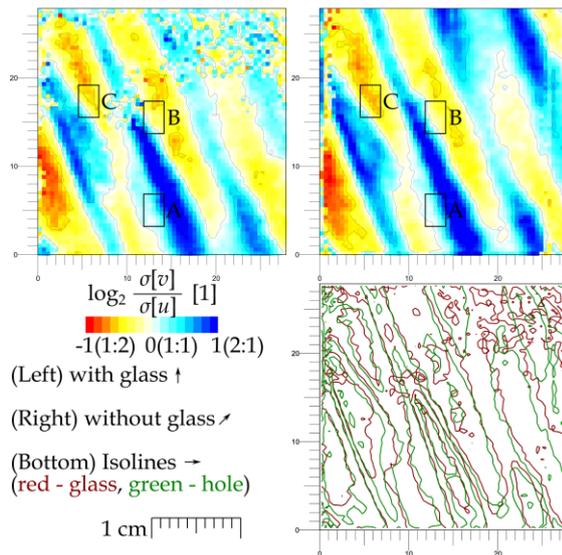
Figure 13: Anisotropy of fluctuations in light of ratio of fluctuations in the tangential to the axial direction [4]. Ignore the point noise in disturbed areas (white spots in Figure 12). The data are taken at tip radius at Mach number Ma = 0.40 and at overloaded regime with wheel-to-fluid ratio 0.40.

We selected different regions of interest according to the same key as above. These regions are located at the lowest velocity magnitude (A), which can be interpreted as a cross-section point of wake past stator with wake past rotor; second is located at the highest velocity magnitude (B), which we interpret as cross-section of stator and rotor jets and the last region is located at low turbulence intensity. The distribution of tangential velocities at these regions is plotted in Figure 14.
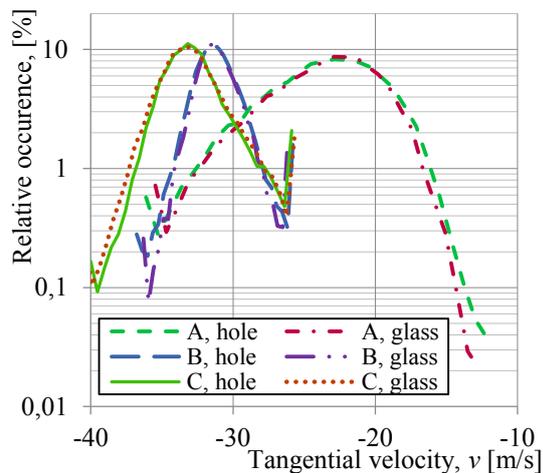

Figure 14: Histogram of instantaneous tangential velocities. The first and last point of each line contains events out of the interval. Datalines associated with glass contains 24000 datapoints, while that of hole consist of 23920 points.

CONCLUSION

By using Particle Image Velocimetry technique, we studied the flow at the output of a single-stage axial turbine at the tip radius. There occurred troubles with oil droplets splashed on the glass window decreasing significantly the quality of data preventing any deeper analysis. We "solved" this problem by removing this problematic glass and in this contribution we show on the available data, that the error caused by this geometry change is more than redeemed by the increase of data quality. Higher discrepancy is observed in the magnitude of average velocity, while the turbulence statistics seem to be unaffected by this change.

Thanks for reading!

ACKNOWLEDGMENTS

REFERENCES

[1] C. Tropea, A. L. Yarin, and J. F. Foss, "Springer handbook of experimental fluid mechanics" (2007)

[2] S. B. Pope, "Turbulent flows" (2000)

[3] G. I. Ilieva, "A deep insight to secondary flows", Deflect and Diffusion Forum **379**, 83 – 107 (2017)

[4] G. P. Romano "Large and small scales in a turbulent orifice round jet: Reynolds number effects and departure from isotropy", International Journal of Heat and Fluid Flow **83**, 108571 (2020)

[5] S. Dutta, P. K. Panigrahi, K. Muralidhar, Journal of Engineering Mechanics **134**, 788 (2008)

[6] M. K. Chauhan, S. Dutta, B. K. Gandhi, Journal of Wind Engineering and Industrial Aerodynamics **184**, 342 (2019)

[7] J. L. Lumley, G. R. Newman, "The return to isotropy of homogeneous turbulence", Journal of Fluid Mechanics **82**, 161-178 (1977)

[8] D. Duda, V. Uruba, "Spatial Spectrum From Particle Image Velocimetry Data", ASME J of Nuclear Rad Sci. **5**, 030912 (2019)